SCIENTIFIC REPORTS

OPEN

SUBJECT AREAS:
SURFACES, INTERFACES AND THIN FILMS
TWO-DIMENSIONAL MATERIALS
CHEMICAL PHYSICS
TOPOLOGICAL INSULATORS

Received
8 April 2013

Accepted
8 August 2013

Published
23 August 2013

Correspondence and requests for materials should be addressed to I.K.S. (phiksou@ust.hk)

Surface Reactivity Enhancement on a Pd/Bi_2Te_3 Heterostructure through Robust Topological Surface States

Qing Lin He[2,3], Ying Hoi Lai[2,3], Yao Lu[1], Kam Tuen Law[1] & Iam Keong Sou[1,2,3]

[1]Department of Physics, The Hong Kong University of Science and Technology, Hong Kong, SAR China, [2]William Mong Institute of Nano Science and Technology, The Hong Kong University of Science and Technology, Hong Kong, SAR China, [3]Nano Science and Technology Program, The Hong Kong University of Science and Technology, Hong Kong, SAR China.

We present a study of the surface reactivity of a Pd/Bi_2Te_3 thin film heterostructure. The topological surface states from Bi_2Te_3, being delocalized and robust owing to their topological natures, were found to act as an effective electron bath that significantly enhances the surface reactivity of palladium in the presence of two oxidizing agents, oxygen and tellurium respectively, which is consistent with a theoretical calculation. The surface reactivity of the adsorbed tellurium on this heterostructure is also intensified possibly benefitted from the effective transfer of the bath electrons. A partially inserted iron ferromagnetic layer at the interface of this heterostructure was found to play two competing roles arising from the higher-lying *d*-band center of the Pd/Fe bilayer and the interaction between the ferromagnetism and the surface spin texture of Bi_2Te_3 on the surface reactivity and their characteristics also demonstrate that the electron bath effect is long-lasting against accumulated thickness of adsorbates.

Being characterized by their gapless topological surface states (TSSs), topological insulators (TIs) are a newly discovered class of quantum-state matter that is characterized by a finite energy bulk gap and Dirac-cone energy dispersion with helical spin texture[1–3]. Owing to this peculiar spin texture, the massless Dirac electrons in TIs are insensitive to spin-independent scattering, which results in protection from nonmagnetic backscatters and localization, endowing TIs with promise for exploring fundamental physics, spin-based electronics and fault-tolerant information processing. The TSSs cannot be destroyed by surface passivation or nonmagnetic imperfections because the topological properties are fully protected by the time-reversal symmetry[4] (TRS). They are robust and essentially persistent despite altering the crystalline shape and orientation, or even disordering the bulk[5]. This is different from the conventional surface states that originated from the surface termination of a material, which is typically fragile and vulnerable to surface defects and contamination. Theoretically, the topological nature of the surface states in three-dimensional (3D) TIs[6] can only be destroyed by magnetic doping to the bulk or adding magnetic impurities on the surface to open up a surface band gap. To date, a number of bismuth- and chalcogen- based binary and ternary semiconductor compounds[7,8], such as Bi_2Te_3, Bi_2Se_3 and Bi_2Te_2Se, have been theoretically predicted to be 3D TIs, which are being widely explored experimentally due to their simple surface-band-structure[9–11]. Recently, based on first-principles density-functional theory calculations, Chen *et al.*[12] proposed a novel application of 3D TIs in heterogeneous catalysis. Their calculations show that the TSSs effectively act as an electron bath, making oxygen and carbon monoxide molecules more prone to dissociate and get adsorbed on a gold-covered Bi_2Se_3 structure through enhancing the molecular adsorption energies. These findings may pave the way for novel applications in surface science, gas sensing and catalysis. In this article, we present results of experimental studies on a similar structure, palladium-covered Bi_2Te_3, focusing on the variation of the surface reactivity under the influence of TSSs, which are consistent with Chen *et al.*'s theoretical predictions. We have also investigated the relevant impact of a ferromagnetic layer deposited at the interface of this heterostructure on its surface reactivity, further confirming our observed enhancement in surface reactivity is originated from the facilitation of delocalized surface electrons of Bi_2Te_3.

Results

The oxidation of Pd thin films on different underlying materials was firstly studied using Sample #1 [S#1, inset of Fig. 1(g) shows its structure] in which a 78-nm-ZnSe buffer was firstly grown on a GaAs (111)B substrate

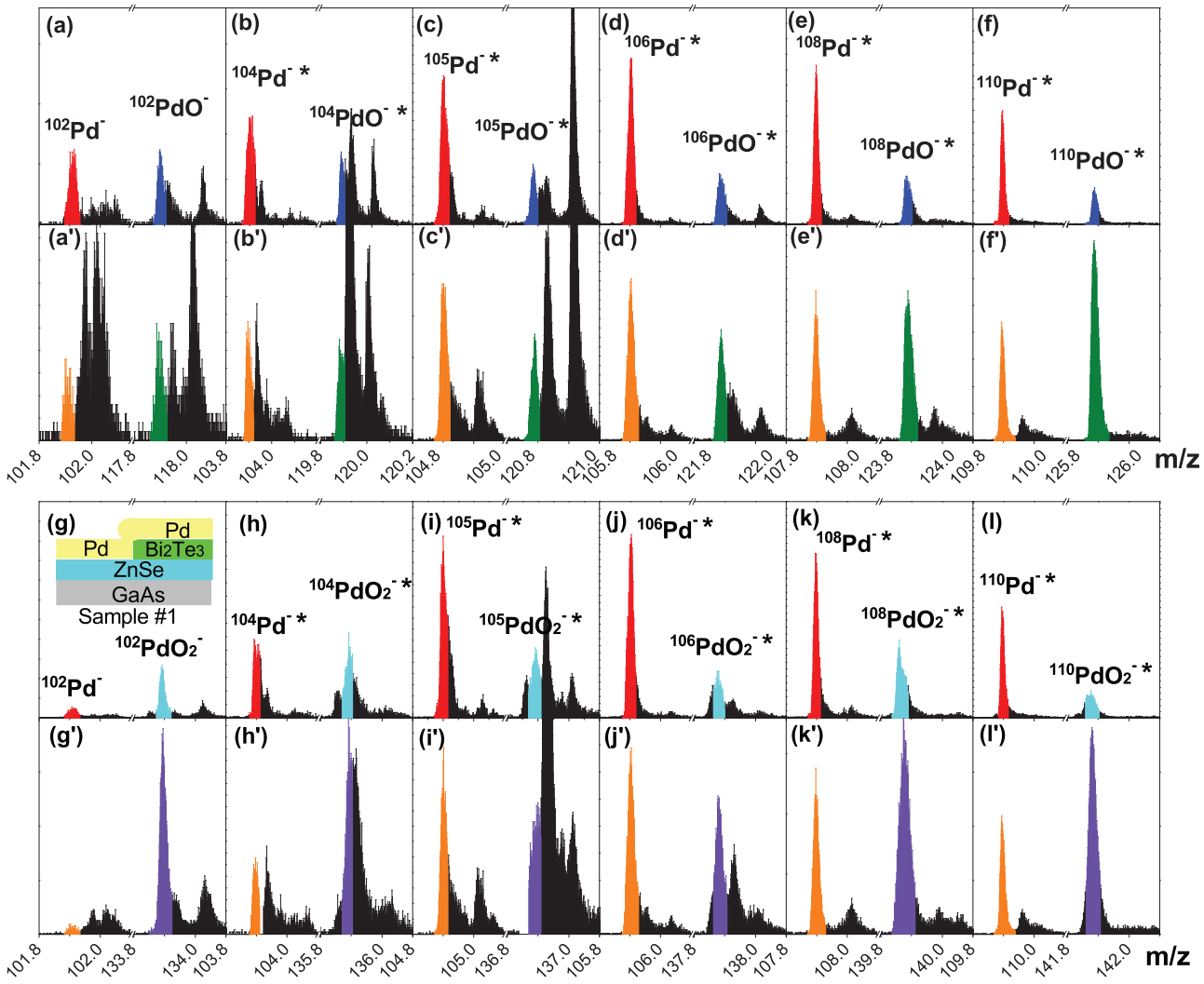

Figure 1 | Partial ToF-SIMS spectra of S#1 in negative polarity obtained from the regions W/O BT and W/BT after exposing the sample in dry air for 3 days. Only the data in the neighborhoods of Pd-, PdO^- and PdO_2^- for each of the isotopic masses of Pd, covering 102, 104, 105, 106, 108 and 110 m/z, are displayed. The inset of (g) displays the structure of S#1. (a)–(f) and (g)–(I) show the data obtained from the region W/O BT, while (a')–(f') and (g')–(l') are those obtained from the region W/BT. The peaks marked with asterisks (*) reflect their mixed compositions with Pd-related hydrides and hydroxides. The intensities of the peaks of the spectra are on linear scale. All the Pd isotope peaks obtained from the region W/O BT and their corresponding peaks obtained from the region W/BT are normalized to the same intensity for clear comparisons.

followed by a deposition of 7-nm-Bi_2Te_3 on half of the ZnSe buffer and a 9-nm-Pd capping layer on the entire surface. S#1 was exposed to dry air for 3 days prior to the measurements of Time-of-Flight Secondary Ion Mass Spectrometry (ToF-SIMS). Fig. 1 displays the resulted ToF-SIMS spectra in the neighborhood of Pd^-, PdO^- and PdO_2^- spectra for each of the isotopic masses of Pd covering 102, 104, 105, 106, 108 and 110 m/z. Fig. 1(a)–(f) and (g)–(l) show the spectra obtained from the region without Bi_2Te_3 (W/O BT) while (a')–(f') and (g')–(l') are those from the region with Bi_2Te_3 (W/BT), respectively. The signals marked in black in Fig. 1 are contributed from organic ions. It is obvious that these organic signals resulted from the region W/BT are much higher than those from the region W/O BT. This indicates that the BT thin film plays a role in enhancing the adsorption of organics on the surface of Pd. However, since the spectra of organic ions are too complicated to be analyzed as they are resulted from numerous organic species existed in ambient air, they are excluded from further analysis. A detailed study was carried out on signals resulted from ions of elemental Pd and inorganic Pd compounds, which includes candidates of PdH^-, PdH_2^-, PdO^-, $PdOH^-$, $PdOH_2^-$, PdO_2^-, PdO_2H^- and $PdO_2H_2^-$.

As can be seen in Fig. 1, signals resulted from ions of elemental Pd and inorganic Pd compounds can be well distinguished from neighboring signals contributed by organic ions, and they are highlighted with different colors. For Pd isotopes with mass of 104 and higher, their nominal Pd^-, PdO^- and PdO_2^- signals may have been superposed by hydrides and hydroxides of Pd. This is why the corresponding peaks shown in Fig. 1 are marked with asterisks (*) to reflect their mixed compositions. Fig. 1 clearly shows that the intensity ratios of PdO^-*/Pd^-* and PdO_2^-*/Pd^-* in the region W/BT are consistently higher than those in the region W/O BT for each of the isotopic masses of Pd. Though these signals are superposed by hydrides and hydroxides of Pd, this observation also qualitatively implies that the underlying BT thin film enhances the oxidation of Pd through efficiently adsorbing oxygenic and hydric clusters. A stronger evidence of this enhancement comes from the signals of $^{102}Pd^-$, $^{102}PdO^-$ and $^{102}PdO_2^-$ as shown in Fig. 1(a), (a'), (g) and (g') since they do not suffer from isotopic superposition. These spectra clearly display that the intensity ratios of $^{102}PdO^-/^{102}Pd^-$ and $^{102}PdO_2^-/^{102}Pd^-$ in the region W/BT are higher than those in the region W/O BT.

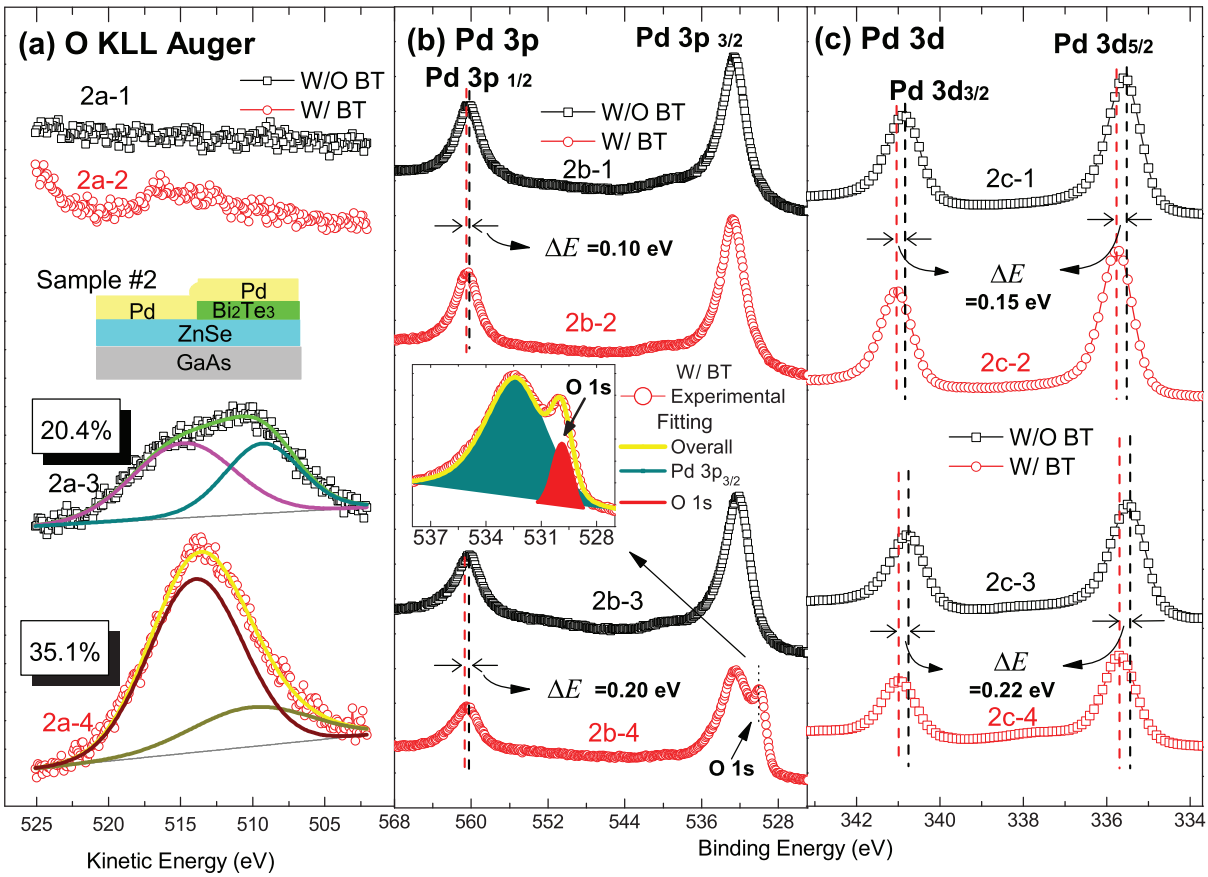

Figure 2 | XPS core-level and Auger spectra of S#2. (a) O KLL Auger peaks. Spectra (2a-1) and (2a-2) are O KLL spectra obtained from the region W/O BT and W/BT of S#2A, while Spectra (2a-3) and (2a-4) are the corresponding spectra obtained from S#2B, respectively. The inset displays the structure of S#2. (b) Pd 3p peaks. Spectra (2b-1) and (2b-2) are Pd 3p spectra obtained from the region W/O BT and W/BT of S#2A, while Spectra (2b-3) and (2b-4) are the corresponding spectra obtained from S#2B, respectively. The inset shows the fitting results of Pd $3p_{3/2}$ and O 1s core-levels in Spectrum (2b-4). (c) Pd 3d peaks. Spectra (2c-1) and (2c-2) are Pd 3d spectra obtained from the region W/O BT and W/BT of S#2A, while Spectra (2b-3) and (2b-4) are the corresponding spectra obtained from S#2B, respectively. All the core-level BE shifts obtained from the regions W/BT and W/O BT are illustrated by dash lines.

A sample [S#2, inset of Fig. 2(a) shows its structure] fabricated with its structure identical to those of S#1 was studied using X-ray photoelectron spectroscopy (XPS) to further reveal the role of the underlying BT thin film on the surface reactivity of Pd layer. XPS could provide more quantitative and direct analysis on the oxidation of Pd and is also able to study the electron transfer by probing the chemical shift of the electronic structure of the elements involved. One piece of this sample (S#2A) was cut and transferred to the XPS system right after being unloaded from the molecular beam epitaxy (MBE) system, while another piece was exposed in dry air for 3 days (S#2B) before being loaded into the XPS system. The resulted O KLL Auger spectra of S#2A are displayed in Fig. 2(a), which show that no notable O KLL signal can be detected in the region W/O BT (Spectrum 2a-1) while a weak O KLL peak can be seen in the spectrum obtained from the region W/BT (Spectrum 2a-2). This difference in peak intensity is even more obvious in the resulted O KLL peaks of S#2B (Spectra 2a-3 and 2a-4). Standard quantitative composition analysis reveals that the atomic concentration of O in percentage in the region W/BT (35.1%) is higher than that of W/O BT (20.4%), while the corresponding O/Pd ratios are 0.209 and 0.108. As shown in Spectra (2a-3) and (2a-4) in Fig. 2(a), each of the resulted O KLL spectra from the regions W/O BT and W/BT can be deconvoluted into two components. The peaks at 509.5 eV on Spectrum (2a-3) and 509.7 eV on Spectrum (2a-4) mainly originate from the standard O Auger KLL transition[13], which involves contributions from O 1s and 2p atomic orbitals. Titkov *et al.*[14] studied the oxidation of pure Pd samples with different amount of adsorbed oxygen and under various heating temperatures using the XPS technique. Their results indicate that the kinetic energy of PdO-related O Auger peak decreases with the increase of the degree of oxidation of Pd, ranging from 514.7 to 513.1 eV for a sample mildly heated under a moderate concentration of O_2 to a sample heated at an elevated temperature under a high concentration of O_2 respectively. Thus, the peaks at 514.9 eV on Spectrum (2a-3) and 513.4 eV on Spectrum (2a-4) are believed to be PdO-related O Auger peaks that correspond to when Pd is weakly and strongly oxidized respectively. The above observations show that Pd underwent a stronger oxidation in the region W/BT than in the region W/O BT. This also can be concluded from the resulted Pd 3p and 3d core-level spectra shown in Fig. 2(b) and (c). Spectra (2b-1) and (2b-2) show the Pd 3p core-level spectra from the regions W/O BT and W/BT of S#2A while Spectra (2c-1) and (2c-2) show the Pd 3d core-level spectra from the corresponding regions. The corresponding spectra of S#2B are shown in Spectra (2b-3), (2b-4), (2c-3) and (2c-4), respectively. As illustrated in Fig. 2(b) and (c), the binding energies (BEs) of Pd $3p_{1/2}$, $3d_{3/2}$ and $3d_{5/2}$ core-levels in the spectra of S#2A obtained from the region W/BT shift positively by 0.10, 0.15 and 0.15 eV respectively in reference to those obtained from the region W/O BT. These shifts are even larger (0.20, 0.22 and 0.22 eV, respectively) in S#2B. Since the core-level BE increases with the oxidation state of metal atoms when a metal is oxidized, these shifts further support that the oxidation of Pd is enhanced by the underlying BT thin film. Referring back to the Pd

$3p_{3/2}$ core-level, its BE is in the neighborhood of that of O 1s [see Fig. 2(b)], and if the oxidation of Pd is not significant, it will be difficult to distinguish the contributions from Pd $3p_{3/2}$ and O 1s, just like what can be seen in Spectra (2b-1), (2b-2) and (2b-3). However, in Spectrum (2b-4) that is obtained from the region W/BT of S#2B, the O 1s peak appears to be well distinguished from the Pd $3p_{3/2}$ peak, which is attributed to a much stronger oxidation of Pd comparing to that of the region W/O BT. The corresponding fitting for the O 1s core-level in Spectrum (2b-4) as shown in the inset of Fig. 2(b) indicates that its BE peak locates at 530.2 eV, which is consistent with the BE range of O 1s (530.1–530.3 eV) reported for a PdO sample[14]. The signature of the O 1s core-level described above acts as another strong evidence that the underlying BT thin film could significantly enhance the oxidation of Pd.

Sample #3 [S#3, inset of Fig. 3(a) shows its structure] was fabricated by *in situ* thermally evaporating Te with nominal thickness of 1.3 nm onto the entire surface of a structure identical to that of S#1. Te is a congener of O and thus can also act as an oxidizing agent for the metallic Pd. The findings obtained from the studies on S#1 and S#2 as described above indicate that the Pd layer in the region W/BT enjoys a stronger surface reactivity as compared with its counterpart in the region W/O BT. Thus, it is expected that more Te will be deposited on the Pd layer in the region W/BT of S#3. One piece of S#3 was cut and transferred to the XPS system right after the sample was unloaded from the MBE system (S#3A), while another piece was exposed in dry air for 3 days before being loaded into the XPS system (S#3B). A quantitative XPS analysis performed on S#3A shows that the surface concentration of Te and the concentration ratio of Te/Pd in the region W/O BT are 33.74% and 0.519. The corresponding data for the region W/BT can be obtained by subtracting the Te contribution of the underlying BT thin film from the apparent XPS data. Using the detected Bi concentration in the region W/BT of S#3A (3.55%) and the detected Bi/Te ratio of S#2A (0.72), the Te contributed from the underlying BT thin film of S#3A was estimated to be 4.93%. With this subtraction carried out, the actual surface concentration of Te and the concentration ratio of Te/Pd in the region W/BT of S#3A are determined to be 42.73% and 0.726, which are indeed substantially higher than those data obtained from the region W/O BT. The chemical shifts of the core-level peaks of Te 3d and Pd 3d resulted from the XPS spectra of S#3A act as another evidence that the surface reactivity of Pd is enhanced by the underlying BT thin film. In Fig. 3(a), Spectra (3a-1) and (3a-2) show the Te 3d core-level spectra in the region W/O BT and W/BT of S#3A, while in Fig. 3(b), Spectra (3b-1) and (3b-2) show the Pd 3d core-level spectra in the corresponding regions, respectively. As shown in Spectra (3a-1) and (3a-2), the Te 3d core-levels in the region W/BT of S#3A negatively shift (corresponding to a stronger reduction for non-metals) by 0.35 eV in reference to those in the region W/O BT, while the corresponding Pd 3d core-levels positively shift (corresponding to a stronger oxidation for metals) by 0.10 eV. The results just described above for S#3A together with the findings obtained from the studies of S#1 and S#2 addressed in the previous two paragraphs all demonstrate that the surface reactivity of Pd in the region W/BT is enhanced by the underlying BT thin film, which is believed to be attributed to the electron bath effect. This effect is mainly due to the facilitation of delocalized surface electrons originated from the TSSs of BT as described in Chen *et al.* 's theoretical model[12]. As the adsorption begins, the surface electrons migrate to the absorbates due to their topological delocalization, which promotes O_2 molecules or Te_n clusters toward dissociative adsorption on Pd.

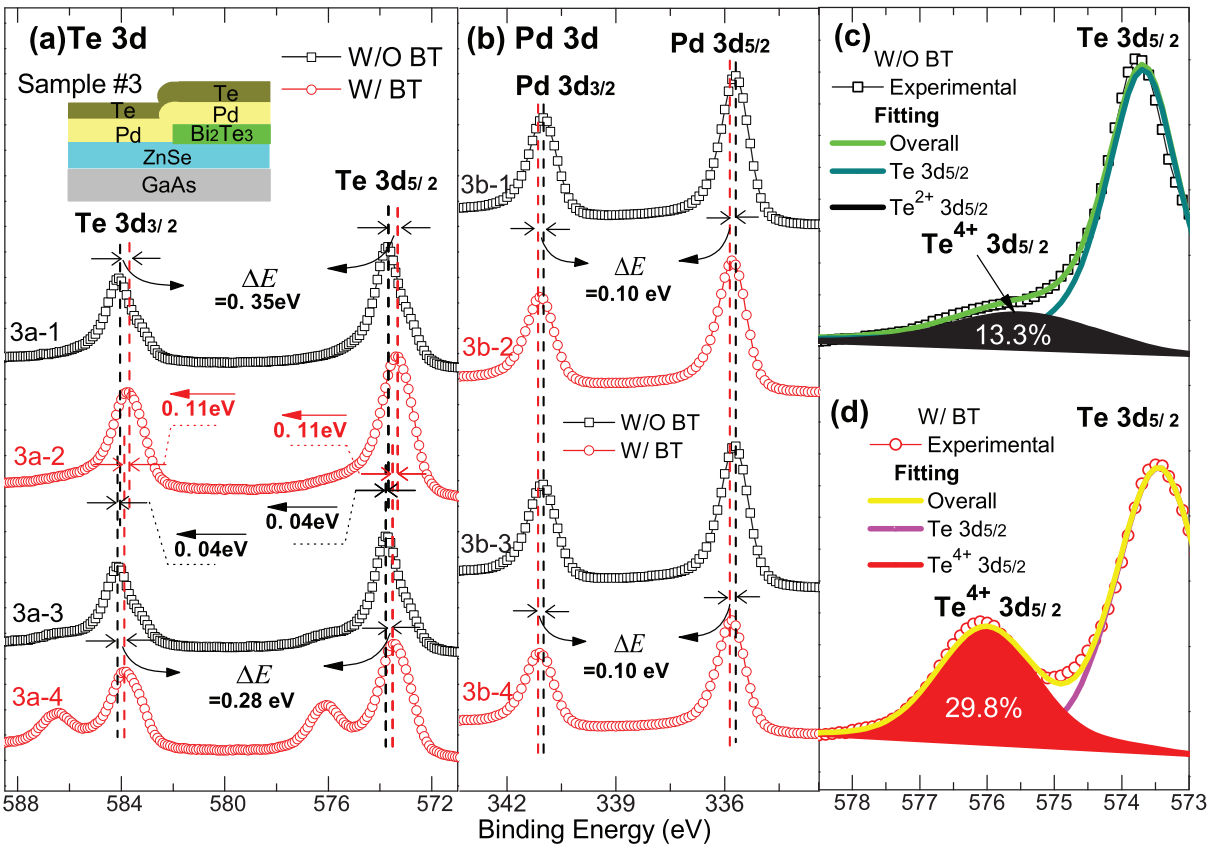

Figure 3 | XPS core-level spectra of S#3. (a) Te 3d peaks. Spectra (3a-1) and (3a-2) are Te 3d spectra obtained from the region W/O BT and W/BT of S#3A, while Spectra (3a-3) and (3a-4) are the corresponding spectra obtained from S#3B, respectively. The inset displays the structure of S#3. (b) Pd 3d peaks. Spectra (3b-1) and (3b-2) are Pd 3d spectra obtained from the region W/O BT and W/BT of S#3A, while Spectra (3b-3) and (3b-4) are the corresponding spectra obtained from S#3B, respectively. (c) and (d) are the fitting results of Te $3d_{5/2}$ peaks in Spectra (3a-3) and (3a-4).

In Fig. 3(b), Spectra (3b-3) and (3b-4) display the Pd 3d core-level spectra in the region W/O BT and W/BT of S#3B. No detectable difference between these spectra and the corresponding spectra of S#3A shown in Spectra (3b-1) and (3b-2) is observed, which can be concluded by their same chemical shift of 0.10 eV. This indicates that the Pd layer is well protected by the Te capping layer against its further reaction with ambient air. In Fig. 3(a), Spectra (3a-3) and (3a-4) display the Te 3d core-level spectra in the region W/O BT and W/BT of S#3B. It can be seen that both the Te 3d core-levels in Spectrum (3a-3) show a positive shift of 0.04 eV relative to Spectrum (3a-1) and barely detectable peak arising on the high-BE shoulder of each Te 3d core-level, while the corresponding shift between Spectra (3a-4) and (3a-2) is 0.11 eV and a well-separated peak appears on the high-BE shoulder of each Te 3d core-level in Spectrum (3a-4). This larger chemical shift implies that the top surface of the Te layer in the region W/BT of S#3B undergoes a stronger oxidation after the sample is exposed in ambient air for 3 days as compared with its counterpart in the region W/O BT. The BEs of these additional peaks on the high-BE shoulders of the Te 3d core-levels match those of the well-known Te^{4+} 3d core-levels arising from the oxidation of Te[15]. A standard data fitting for Spectra (3a-3) and (3a-4) in the spectral regions involving the Te and Te^{4+} $3d_{5/2}$ core-levels is carried out to determine the percentage concentration of Te^{4+} relative to the total amount of Te with the results shown in Fig. 3(c) (13.3%) and (d) (29.8%), respectively. The observations of a larger chemical shift of Te 3d core-levels and a significantly higher percentage concentration of Te^{4+} in the region W/BT of S#3B indicate the surface reactivity of the Te layer in this region is also intensified. As Te has a semimetallic conductivity, a possible explanation for this behavior is that the top surface of the Te layer also gets a share of the surface electrons transferred out of the TSSs of the underlying BT thin film.

The above experimental observations are consistent with a hypothesis that the TSSs can penetrate the 9-nm-Pd layer and extend to its surface. We have performed theoretical calculation using a standard tight-binding model constructed for the Pd/Bi_2Te_3 bilayer. It is found that the TSSs can strongly hybridize with the metal states and form standing waves in the metal, which can extend to the surface of the metal even under a strong disorder. The details of this theoretical work can be found in the Supplementary Information.

As predicted by theories[16,17] and proved by recent experiments[18–20], a deposition of ferromagnetic impurities on a TI surface will lead to an interaction between the ferromagnetism and the surface spin texture of TI , which breaks the TRS and opens up a surface band gap in the energy spectrum of TSSs. Consequently, this will lead to a transition of the Dirac electrons of TSSs from being massless and delocalized to massive and localized. Thus, by inserting an Fe thin layer at the interface between Pd and BT of a Te/Pd/BT structure, one can study the expected weakening of the enhancement in the surface reactivity of Pd and Te so as to further confirm the role of BT in

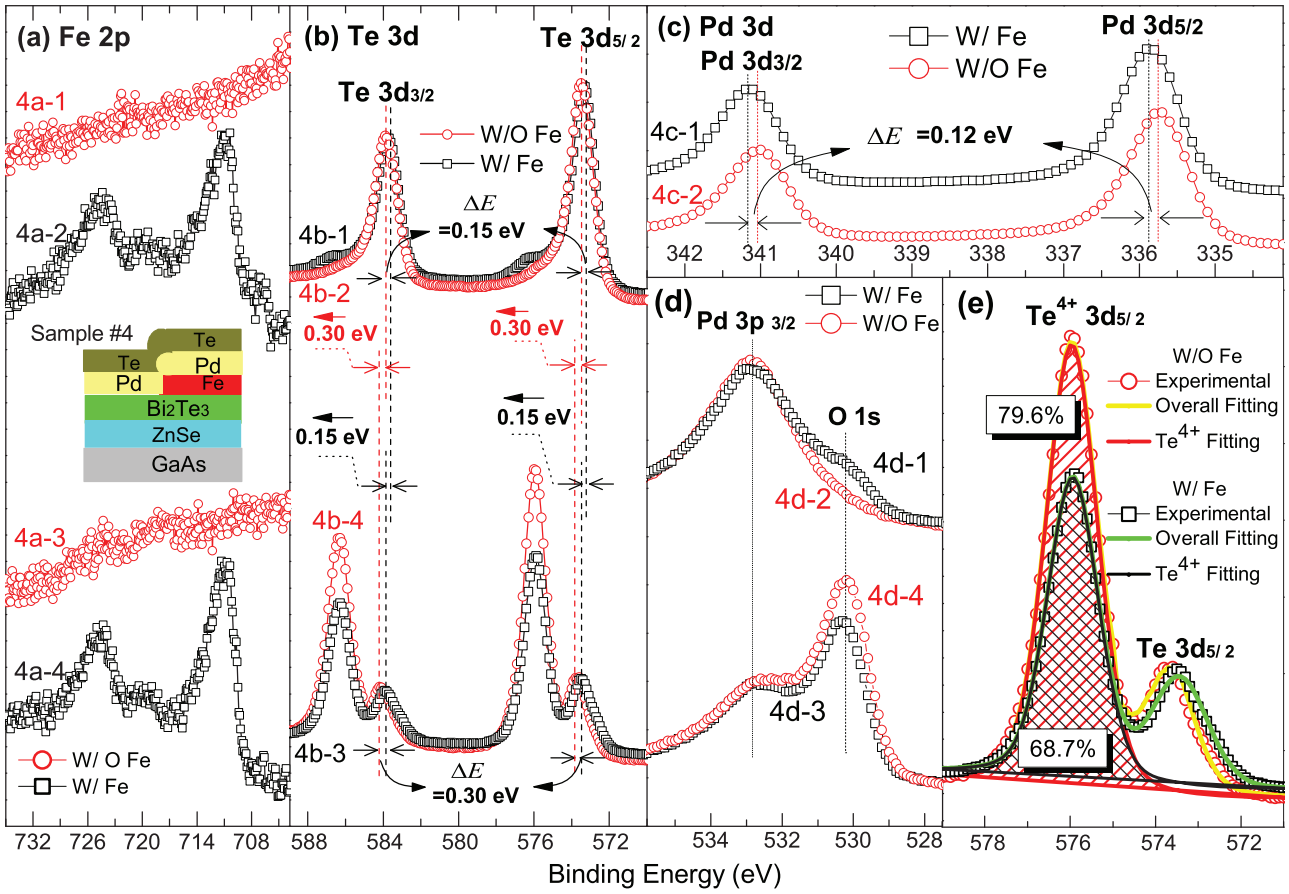

Figure 4 | XPS core-level spectra of S#4. (a) Fe 2p peaks. Spectra (4a-1) and (4a-2) are the Fe 2p core-levels spectra obtained from the region W/O Fe and W/Fe of S#4A, while Spectra (4a-3) and (4a-4) are the corresponding spectra obtained from S#4B, respectively. The inset displays the structure of S#4. (b) Te 3d peaks. Spectra (4b-1) and (4b-2) are Te 3d core-levels spectra obtained from the region W/Fe and W/O Fe of S#4A, while Spectra (4b-3) and (4b-4) are the corresponding spectra obtained from S#4B, respectively. (c) Pd 3d peaks. Spectra (4c-1) and (4c-2) are the Pd 3d core-levels spectra obtained from the region W/Fe and W/O Fe from S#4A. (d) Pd 3p and O 1s peaks. Spectra (4d-1) and (4d-2) are the spectra in a spectral region involving the Pd 3p and O 1s core-levels obtained from the region W/Fe and W/O Fe of S#4A, while Spectra (4d-3) and (4d-4) are the corresponding spectra obtained from S#4B, respectively. (e) Fitting results of Te $3d_{5/2}$ peaks in Spectra (4b-3) and (4b-4).

providing the electron bath. Sample #4 [S#4, inset of Fig. 4(a) shows its structure] was fabricated with a 78-nm-ZnSe buffer layer and a 7-nm BT thin film on the entire surface followed by depositing 2-monolayers of Fe on half of the BT surface, and then covered the entire sample surface with a 9-nm-Pd layer then a 1.3-nm-Te layer. An as-prepared piece of this sample (S#4A) was quickly transferred to the XPS system and another piece was kept in dry air for 7 days (S#4B) prior to performing the XPS measurement. The resulted spectra in the spectral region of the Fe 2p core-levels are shown in Fig. 4(a), in which Spectra (4a-1) and (4a-2) are obtained from the region without Fe (W/O Fe) and with Fe (W/Fe) of S#4A, while the corresponding spectra of S#4B are shown as Spectra (4a-3) and (4a-4). As expected, no detectable Fe signal was resulted in Spectra (4a-1) and (4a-3), while Spectra (4a-2) and (4a-4) display the signature of the expected Fe 2p core-levels spectra. It is worth to note that Spectra (4a-2) and (4a-4) are basically identical, indicating the inserted Fe layer is quite stable.

According to the *d*-band theory[21], the surface reactivity of a metal largely depends on its electronic states in the entire valence band. The surface reactivity of a metal will increase along with the rising of the position of the average energy of its *d*-band, the so-called *d*-band center. Referring to the values of the *d*-band centers of surface overlayers relative to clean metals in Ref[22], the Pd/Fe bilayer has a higher-lying *d*-band center (−1.32 eV) than that of a pure Pd (−1.83 eV). Thus, the surface reactivity of the Pd/Fe bilayer in the region W/Fe of S#4 is expected to be more active than that of elemental Pd in the region W/O Fe by considering the effect arising from the insertion of Fe alone. However, the underlying BT thin film across the whole sample is also expected to enhance the surface reactivity of the Pd layer though this effect in the region W/Fe will be significantly diminished due to the breaking of TRS by the Fe ferromagnetic layer as described above. Thus, the insertion of Fe in S#4 is playing two competing roles in affecting the surface reactivity of Pd. However, the active periods of these roles may depend on each role's ability in extending through the adsorbates of which their thicknesses are accumulated with time. After exposing S#4 in dry air, as the thickness of the Te-oxide layer, which is highly insulating, increases with time, the role of the *d*-band center of the Pd/Fe active bilayer will be

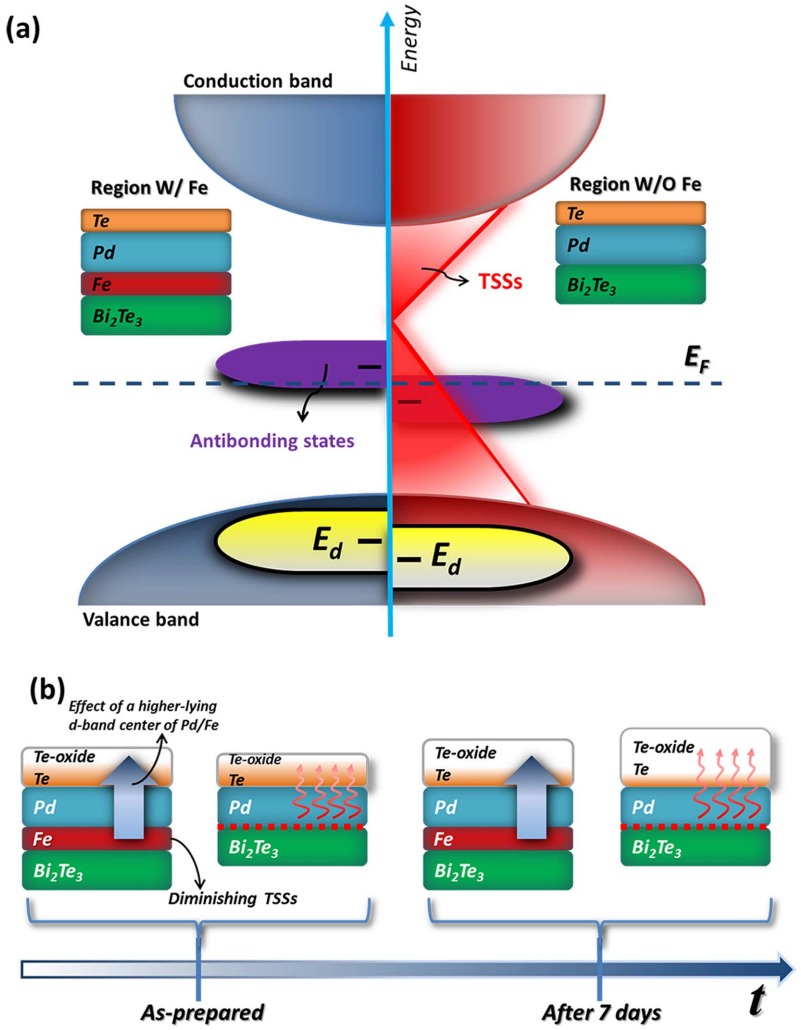

Figure 5 | Schematic illustrations of the energy band structures and the temporal evolvements of the oxidation of Te of S#4 under the impacts of a higher-lying *d*-band center [for the region W/Fe (left)] and the TSSs [for the region W/O Fe (right)]. (a) The interaction between the adsorbates and the *d* electrons on the surface of Pd causes an upswing of the energy of the *d*-band center, E_d, leading to split-off bonding and antibonding states in the energy spectrum[22]. The upshifted antibonding states above the Fermi level E_F become mostly empty, which enhances the surface adsorption. The upward shift of the TSSs in the region W/O Fe indicates that the surface electrons are transferred out of the TSSs, which promotes the Te_n clusters and O_2 molecules toward dissociative adsorption on Pd[12]. (b) The temporal evolutions of the oxidation of Te in the region W/Fe and W/O Fe under the effect of a higher-lying *d*-band center of Pd/Fe and the TSSs respectively. The arrows shown in this diagram represent the high-lying *d*-band effect (blue) and the extending of the surface electrons (red).

weakened. On the other hand, as recently predicted by Wu *et al.*[23], when a certain conventional insulator (CI) overlayer is deposited onto a TI surface, the TSSs may float to the top of the CI overlayer through a nontrivial topological phase transition of the CI. Thus, the electrons contributed from the electron bath of the underlying BT thin film in the region W/O Fe of S#4 might still partially tunnel through the accumulating Te-oxide layer, providing a long-lasting enhancement of the surface reactivity in contrast to the role of the higher-lying *d*-band center in the region W/Fe.

The resulted XPS Te 3d core-level spectra obtained from the region W/Fe and W/O Fe of S#4A are shown as Spectra (4b-1) and (4b-2) in Fig. 4(b), while the Pd 3d core-level spectra in the corresponding regions are shown as Spectra (4c-1) and (4c-2) in Fig. 4(c). The core-level BEs of the regions W/Fe and W/O Fe of S#4A can be obtained from these spectra to be 573.35 and 573.50 eV for Te $3d_{5/2}$ core-level, and 335.86 and 335.74 eV for Pd $3d_{5/2}$ core-level [the corresponding BE shifts between the regions W/Fe and W/O Fe of S#4A are given in Fig. 4(b) and (c) as 0.15 and 0.12 eV for Te $3d_{5/2}$ and Pd $3d_{5/2}$ respectively]. For S#4A, the observed lower BE of Te $3d_{5/2}$ core-level and the higher BE of Pd $3d_{5/2}$ core-level in the region W/Fe in reference to those in the region W/O Fe imply that the Te/Pd interface in the region W/Fe undergoes a stronger reduction of Te and an oxidation of Pd than that in the region W/O Fe. This observation is consistent with the prediction by the *d*-band theory mentioned above. Furthermore, this effect is also reflected in the stronger oxidation of the surface of Te layer in the region W/Fe of S#4A than that in the region W/O Fe as shown in Spectrum (4b-1) where weak Te^{4+} 3d core-level peaks appear in the former region while they are undetectable in the latter region as shown in Spectrum (4b-2). In fact, Fig. 4(d) also shows that a stronger O 1s core-level appears on the lower-BE shoulder of the Pd $3p_{3/2}$ core-level spectrum resulted from the region W/Fe (Spectrum 4d-1) in S#4A while it is barely detectable in the spectrum obtained from the region W/O Fe (Spectrum 4d-2). All the results of S#4A described above indicate that for a fresh piece of the as-prepared S#4, the role of the higher-lying *d*-band center of the Pd/Fe bilayer in the region W/Fe overwhelms that of the electron bath effect originated from the underlying BT thin film in the region W/O Fe.

However, interestingly, for S#4B that has been exposed to air for 7 days, the characteristics of its resulted Te 3d core-level spectra obtained from the regions W/Fe and W/O Fe [Spectra (4b-3) and (4b-4) in Fig. 4(b)] and its corresponding O 1s core-level spectra [Spectra (4d-3) and (4d-4) in Fig. 4(d)], to be addressed below, show that the oxidation of Te in the region W/O Fe turns to be stronger than that in the region W/Fe. The intensities of Te^{4+} 3d peaks and O 1s peak in Spectra (4b-4) and (4d-4) obtained from the region W/O Fe are higher than those in Spectra (4b-3) and (4d-3) obtained from the region W/Fe. Besides, it can be seen that both the Te 3d core-levels in Spectrum (4b-4) show a positive shift of 0.30 eV relative to those in Spectrum (4b-2), which is larger than the corresponding shift between Spectra (4b-3) and (4b-1) (0.15 eV). Fig. 4(e) shows the results of a standard fitting performed in the spectral region involving the Te $3d_{5/2}$ and Te^{4+} $3d_{5/2}$ core-levels in Spectra (4b-3) and (4b-4) of S#4B, which reveal that the percentage concentration of Te^{4+} relative to the total amount of Te is 79.6% in the region W/O Fe and 68.7% in the region W/Fe respectively.

The experimental results obtained on S#4 as described in the last two paragraphs provide the evidence that though the role of a higher-lying *d*-band center of Pd/Fe win against the electron bath effect from the BT thin film at an initial stage of the enhancement of the surface reactivity, the latter will take over the former at a later stage. This observation in fact can be explained by our previous prediction that the accumulation of Te-oxide will gradually diminish the role of the higher-lying *d*-band center, while the role of the electron bath effect originated from the TI persists assuming the electrons of TSSs can partially tunnel onto the surface of Te-oxide layer. The long-lasting enhancement of the surface reactivity attributed to the facilitation through the electron bath of TSSs may find novel important applications in surface science, gas sensing and catalysis. Fig. 5 illustrates the energy band structures and the temporal evolvements of the oxidation of Te of S#4 under the impacts of a higher-lying *d*-band center and the TSSs, which are based on the experimental results obtained in this work.

To investigate the Pd-thickness dependence of the enhancement of the surface reactivity of the Pd/Bi_2Te_3 heterostructure, XPS analysis was performed on S#5, which is a Pd/Bi_2Te_3 heterostructure containing 3 regions with Pd coverage of 4, 6 and 8 monolayers. An as-prepared piece of this sample (S#5A) was quickly transferred to the XPS system and another piece was kept in dry air for 3 days (S#5B) prior to performing the XPS measurement. A standard data fitting for the resulted Pd $3d_{5/2}$ spectra was carried out to resolve the core-level peaks into Pd and PdO components (see Fig. 6). As the PdO layer always locates on the top surface, the area of the PdO components obtained from the fitting results of the XPS spectra can be taken as a good approximation of the amount of the oxidized Pd. Fig. 6 displays the resulted amount of the oxidized Pd versus the Pd coverage for S#5A and S#5B. If the oxidation of the Pd layers is purely native, one should expect the amount of this oxide would not

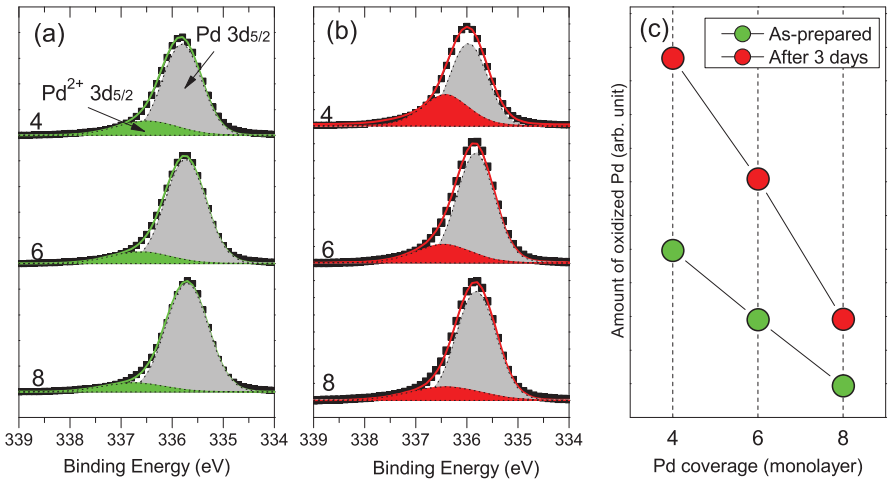

Figure 6 | XPS Pd $3d_{5/2}$ core-level spectra and the resulted amount of oxidized Pd of S#5. (a) and (b) are Pd $3d_{5/2}$ core-level spectra obtained from S#5A and S#5B respectively for three regions with Pd coverage of 4, 6 and 8 monolayers. Also shown in each spectrum are the Pd and PdO peaks resulted from standard XPS fitting. (c) Pd coverage dependence of the amount of oxidized Pd of S#5A and S#5B.

depend on the coverage of Pd. However, as can be seen in Fig. 6(c), both samples show a consistent descending trend for the amount of PdO as the Pd coverage increases, which can be regarded as a signature of the electron bath effect from the TSSs, as one would expect that this effect should normally weaken for a thicker Pd layer in this heterostructure.

Discussion

Through investigating the adsorptions and surface reactions on a Pd/Bi_2Te_3 heterostructure, we present experimental evidences that the electron bath effect provided by the TSSs from the TI thin film can significantly enhance the surface reactivity. The results from ToF-SIMS and XPS reveal that the reactivity of Pd and a Te layer adsorbed on this heterostructure is enhanced by the electron bath effect, which is consistent with our theoretical calculation. A partial insertion of an Fe ferromagnetic layer at the interface between Pd and Bi_2Te_3 layers was used to illustrate the two competing roles arising from the higher-lying *d*-band center of the Pd/Fe bilayer and the interaction between the ferromagnetism and the surface spin texture of Bi_2Te_3 on surface reactivity. Our work also demonstrates the long-lasting nature of the robust TSSs in enhancing the surface reactivity of this heterostructure, which may pave the way for searching and designing new catalysts.

Methods

Sample preparation. All the samples studied in this paper were fabricated on GaAs (111) B semi-insulating substrates by a VG-V80H MBE system. For S#1 and S#2, a 78-nm-ZnSe buffer layer was firstly deposited and then half of the sample was covered by a Ta strip *in situ* followed by the growth of 7-nm Bi_2Te_3 using Bi_2Te_3 compound source. The Ta strip was then removed and the whole sample surface was deposited with a 9-nm-amorphous-Pd overlayer. For S#3, the growth procedures of S#1 were firstly applied followed by a deposition of Te with nominal thickness of 1.3 nm. For S#4, a 78-nm-ZnSe buffer layer and a 7-nm-BT thin film were deposited successively on the entire surface. Then half of the surface was covered by the Ta strip *in situ*, followed by a deposition of Fe of 2-monolayers. 9-nm-amorphous-Pd overlayer was then deposited on the entire surface of the sample, followed by a deposition of Te with nominal thickness of 1.3 nm *in situ*. For S#5, a 78-nm-ZnSe buffer layer was firstly deposited, followed by the growth of 7-nm Bi_2Te_3. Then 4 monolayers of Pd were deposited on the entire surface. About one third of the surface was then covered by the Ta strip, followed by the growth of another 2 monolayers of Pd. The Ta strip was then further moved to cover more area of the surface. After each move, 2 monolayers of Pd were deposited on the remaining exposed surface. At the end of the growth, the resulted sample contains 3 regions with Pd coverage of 4, 6 and 8 monolayers, respectively. All the growth processes were performed in ultra-high-vacuum chambers with a basic pressure better than 2.5×10^{-9} mbar.

ToF-SIMS and XPS measurements. S#1 was exposed to dry air for 3 days prior to the ToF-SIMS experiment. Static SIMS spectra measurements were carried out using a Cameca-IMS 4F ToF-SIMS V spectrometer. Pulsed Bi^{3+} primary ions bombarded the surface of the sample with the resulting ion doses less than 3×10^{11} ions cm^{-2}, ensuring the static SIMS conditions. Two 100×100 μm^2 areas on each of the two specified regions (mentioned in the main text) of the sample were measured and the results were found highly consistent. All the peaks highlighted in the ToF-SIMS spectra were defined through pinpointing the positions of peaks of the ions involved according to the SIMS database with ranges of $\pm 0.03 \sim 0.04$ m/z from the centers of the peaks. All the XPS measurements were performed using Kratos-Axis Ultra DLD XPS *ex situ*. This instrument was equipped with a monochromatic Al kα x-ray source (photon energy 1486.7 eV, 150 W) and the measurements were taken in hybrid lens mode with an energy step of 100.0 meV, a pass energy of 40 eV and a large measuring area of 1×2 mm^2. Two different points on each of the two specified regions of each sample were measured and the results also show high consistency.

1. Hasan, M. & Kane, C. Colloquium: Topological insulators. *Rev. Mod. Phys.* **82**, 3045 (2010).
2. Moore, J. E. The birth of topological insulators. *Nature* **464**, 194 (2010).
3. Qi, X. L. & Zhang, S. C. Topological insulators and superconductors. *Rev. Mod. Phys.* **83**, 1057 (2011).
4. Fu, L. & Kane, C. Topological insulators with inversion symmetry. *Phys. Rev. B* **76**, 045302 (2007).
5. Franz, M. In praise of exact quantization. *Science* **329**, 639 (2010).
6. Fu, L., Kane, C. & Mele, E. Topological insulators in three dimensions. *Phys. Rev. Lett.* **98**, 106803 (2007).
7. Zhang, H. *et al.* Topological insulators in Bi_2Se_3, Bi_2Te_3 and Sb_2Te_3 with a single Dirac cone on the surface. *Nat. Phys.* **5**, 438 (2009).
8. Miyamoto, K. *et al.* Topological surface states with persistent high spin polarization across the Dirac point in Bi_2Te_2Se and Bi_2Se_2Te. *Phys. Rev. Lett.* **109**, 166802 (2012).
9. Kim, D. *et al.* Surface conduction of topological Dirac electrons in bulk insulating Bi_2Se_3. *Nat. Phys.* **8**, 459 (2012).
10. Alpichshev, Z. *et al.* STM Imaging of electronic waves on the surface of Bi_2Te_3: topologically protected surface states and hexagonal warping effects. *Phys. Rev. Lett.* **104**, 016401 (2010).
11. Qu, D. X., Hor, Y. S., Xiong, J., Cava, R. J. & Ong, N. P. Quantum oscillations and Hall anomaly of surface states in the topological insulator Bi_2Te_3. *Science* **329**, 821 (2010).
12. Chen, H., Zhu, W., Xiao, D. & Zhang, Z. CO oxidation facilitated by robust surface states on Au-covered topological insulators. *Phys. Rev. Lett.* **107**, 056804 (2011).
13. Cherepin, V. T. Secondary Ion Mass Spectroscopy of Solid Surfaces (CRC Press,1987).
14. Titkov, A. I., Salanov, A. N., Koscheev, S. V. & Boronin, A. I. Mechanisms of Pd(110) surface reconstruction and oxidation: XPS, LEED and TDS study. *Surf. Sci.* **600**, 4119 (2006).
15. Wagner, C. D. Handbook of x-ray photoelectron spectroscopy: a reference book of standard data for use in x-ray photoelectron spectroscopy (Physical Electronics Division, Perkin-Elmer Corp.) (1979).
16. Abanin, D. A. & Pesin, D. A. Ordering of magnetic impurities and tunable electronic properties of topological insulators. *Phys. Rev. Lett.* **106**, 136802 (2011).
17. Liu, Q., Liu, C. X., Xu, C., Qi, X. L. & Zhang, S. C. Magnetic impurities on the surface of a topological insulator. *Phys. Rev. Lett.* **102**, 156603 (2009).
18. Chen, Y. L. *et al.* Massive Dirac Fermion on the surface of a magnetically doped topological insulator. *Science* **329**, 659 (2010).
19. Wray, L. A. *et al.* A topological insulator surface under strong Coulomb, magnetic and disorder perturbations. *Nat. Phys.* **7**, 32 (2010).
20. He, H. T. *et al.* Impurity effect on weak antilocalization in the topological insulator Bi_2Te_3. *Phys. Rev. Lett.* **106**, 166805 (2011).
21. Anders Nilsson, Pettersson Lars, G. M. & Nørskov, J. K. Chemical Bonding at Surfaces and Interfaces (Elsevier, Amsterdam, 2008).
22. Hammer, B. & Norskov, J. K. Theoretical surface science and catalysis—calculations and concepts. *Adv. in Catal.* **45**, 71 (2000).
23. Wu, G. *et al.* Tuning the vertical location of helical surface states in topological insulator heterostructures via dual-proximity effects. *Sci. Rep.* **3**, 1233; doi:10.1038/srep01233 (2013).

Acknowledgments

We gratefully acknowledge the use of the facilities in the Materials Characterization and Preparation Facility (MCPF) at the Hong Kong University of Science and Technology, and specially thank Nick K. C. HO and Dr. Lutao WENG for their technical assistance in XPS and ToF-SIMS characterization. The work described here was substantially supported by a grant from the Research Grants Council of the Hong Kong Special Administrative Region, China (project No. 604910).

Author contributions

Q.L.H. and I.K.S. designed the experiments. Q.L.H., Y.H.L. and I.K.S. performed the experiments. K.T.L. and Y.L. performed the theoretical calculation. I.K.S. supervised the whole project. Q.L.H. and I.K.S. carried out the data analysis and wrote the manuscript with contribution from K.T.L., Y.L. and Y.H.L.

Additional information

Supplementary information accompanies this paper at http://www.nature.com/scientificreports

Competing financial interests: The authors declare no competing financial interests.

How to cite this article: He, Q.L., Lai, Y.H., Lu, Y., Law, K.T. & Sou, I.K. Surface Reactivity Enhancement on a Pd/Bi_2Te_3 Heterostructure through Robust Topological Surface States. *Sci. Rep.* **3**, 2497; DOI:10.1038/srep02497 (2013).